Adaptive Gain Tuning Rule for Nonlinear Sliding-mode Speed Control of Encoderless Three-phase Permanent Magnet Assisted Synchronous Motor

Ghada A. Abdel Aziz, *Member, IEEE,* and Rehan Ali Khan

***Abstract*—In this paper, an adaptive gain tuning rule is designed for the nonlinear sliding mode speed control (NSMSC) in order to enhance the dynamic performance and the robustness of the permanent magnet assisted synchronous reluctance motor (PMa-SynRM) with considering the parameter uncertainties. A nonlinear sliding surface whose parameters are altering with time is designed at first. The proposed NSMSC can minimize the settling time without any overshoot via utilizing a low damping ratio at starting along with a high damping ratio as the output approaches the target set-point. In addition, it eliminates the problem of the singularity with the upper bound of an uncertain term that is hard to be measured practically as well as ensures a rapid convergence in finite time, through employing a simple adaptation law. Moreover, for enhancing the system efficiency throughout the constant torque region, the control system utilizes the maximum torque per ampere technique. The nonlinear sliding surface stability is assured via employing Lyapunov stability theory. Furthermore, a simple sliding mode estimator is employed for estimating the system uncertainties. The stability analysis and the experimental results indicate the effectiveness along with feasibility of the proposed speed estimation and the NSMSC approach for a 1.1-kW PMa-SynRM under different speed references, electrical and mechanical parameters disparities, and load disturbance conditions.**

***Index Terms*—Permanent magnet assisted synchronous reluctance motor, Nonlinear sliding mode speed control, Speed estimation, Parameter uncertainties, Sliding mode estimator.**

NOMENCLATURE

V_q, V_d, I_q, I_d	The *q*-*d* stator voltages and currents
L_q, L_d	The *q*-*d* stator inductances per phase
V_d^*,V_q^*	The reference *d*-*q* axis voltages
I_d^*,I_q^*	The reference *d*-*q* axis currents
λ_f	The flux linkage of permanent magnet
R	Stator resistance per phase
P	Number of pair-poles
ω_r	The rotor mechanical speed
ω_r^*	The speed command
θ_r	The rotor mechanical position angle
J	The rotor inertia
T_L	The external load torque
F	The damping coefficient

Manuscript received August 15, 2022; revised October 27, 2022; accepted December 09, 2022. Date of publication September 25, 2023; date of current version February 17, 2023.

Ghada A. Abdel Aziz is with the Power Electronics and Energy Conversion Department, Electronics Research Institute, Cairo 11843, Egypt.(e-mail: ghada_ahmed@ieee.org)

Rehan Ali Khan is with the Department of Electrical Engineering, University of Science & Technology, Bannu, Pakistan.

(Corresponding Author: Ghada A. Abdel Aziz)

Digital Object Identifier 10.30941/CESTEMS.2023.00025

I. INTRODUCTION

THANKS to the inherent characteristics of high torque–inertia ratio, rapid control response, high power factor, high efficiency along with high-power density, permanent magnet assisted synchronous reluctance motors (PMa-SynRMs) have been extensively applied in industrial applications, ranging from servo control to traction drives [1]-[3]. Nevertheless, these motors are considered multivariable coupled system and highly nonlinear system as well as their performance can be degraded due to the parameter disparities throughout the motor operation [4]. As the PMa-SynRM rotor flux linkage along with stator resistance change because of magnetic saturation, temperature alteration, along with aging, thus, precise and robust multiparameter estimation and robust control approaches are definitely needed for enhancing the PMa-SynRM operation [5].

In [6], for PMSM, the inductances, flux linkages, along with PM flux linkage have been estimated with core loss compensation. As through the multiple differential measurements, the flux linkage error as a result of core loss can be compensated for enhancing the flux linkage estimation precision. Afterwards, the polynomial-based flux linkage model was employed for deriving cross-saturation inductances along with PM flux linkage. Self-inductances have been estimated from the flux linkage model through utilizing the least-squares approach. In [7], an amplitude-auto-adjusting signal injection approach has been introduced for the PMSM parameter self-learning throughout standstill considering the digital time-delay effect along with inverter nonlinearities. Although this approach fulfilled the inductance identification process with unpredicted rotor rotation throughout the self-commissioning process, there is an expected execution time delay in digital control system of the drive system. In [8], a current injection-based parameter estimation approach with enhanced recursive least square approach have been introduced for dual 3-phase PMSM with considering the magnetic saturation and inverter nonlinearity. Although, this

approach tracked the stator resistance and rotor flux linkage accurately, nevertheless it has a limitation in the estimation of the inductances.

In [9], two Kalman-filter-based online identification approaches have been proposed for PMSM. One has been formulated from an extended Kalman filter (EKF); meanwhile the second one employed a dual EKF. Although, this approach can estimate the stator resistance properly, it has complex algorithmic structure and was insensitive to noise. In [10], an online parameter identification approach has been introduced for PMSM deadbeat control. In this approach, an identification model has been formulated for estimating the PMSM parameter errors from the offsets of the deadbeat control. Afterwards, a parameter perturbation approach has been introduced for collecting the basic data to solve the rank lacking problem in the parameter identification process. Although, the identification approach has better performance in online operation, it is hard to be applied in the practical system because of the high computational burden.

In [11], two offline approaches have been proposed for estimating the PMSM initial rotor position along with phase inductance through the line-to-line voltage injection as well as the stator *dq*-voltage injection. Although the estimated inductance via the proposed approaches did not contain the cross-coupling and saturation effects, the proposed approaches can be utilized for designing the current controllers.

Undesirable mechanical and electrical parameters variations of the permanent magnet synchronous motors can pose risks to the connected power conversion systems and deteriorate the control response. Thus, for enhancing the robustness of permanent magnet synchronous motors control, different control approaches have been introduced.

In [12], a robust discrete-time predictive current control approach for the PMa-SynRM has been introduced. This controller has a discrete-time integral term, which has been added to the traditional deadbeat current predictive control for enhancing the stability and robustness of the PMa-SynRM currents. Although the proposed controller approach was robust to acute the PMa-SynRM parameters disparities, it relies on the model accuracy. In [13], a robust control approach with parametric adaptation has been proposed for PMSM, which includes a disturbance-observer-based speed controller along with adaptive robust current controller. Although this controller fulfilled robust regulations of rotor speed and stator currents and estimated properly the stator resistance, flux linkage of the permanent magnet, along with stator inductance, it has complex structure and hard to be applied in the industrial applications. In [14], a new sliding mode speed controller has been introduced for the parallel operation of dual PMSMs with a single inverter. This controller had robust control performance along with stable operation in the steady state as well as the transient state. However, it needs a load torque estimator for determining which motor is the master one. In [15], a discrete compound integral terminal sliding mode control has been introduced for PMSM. The integral terminal sliding mode control (SMC) is utilized for realizing the state convergence in finite time. And an extended state estimator-based compensator is utilized for solving the problem that SMC requires large switching gain for handling the disturbances. This controller has excellent disturbance rejection ability and model adaptability. However, for the high-frequency disturbance, the efficacy of this controller will not be assured.

This paper aims to enhance the low speed response of the PMa-SynRM through utilizing an adaptive gain tuning rule with the NSMSC for enhancing the dynamic performance and the robustness of a three-phase PMa-SynRM with considering the parameter uncertainties. Fig. 1 illustrates the block diagram of the encoderless PMa-SynRM drive system with the super-twisting sliding mode current controllers (ST-SMCCs) for the *dq*-axis currents, uncertainties estimator, along with the nonlinear sliding mode speed controller (NSMSC) using the space vector pulse width modulation. The detailed design structure of the whole drive system is introduced in this paper.

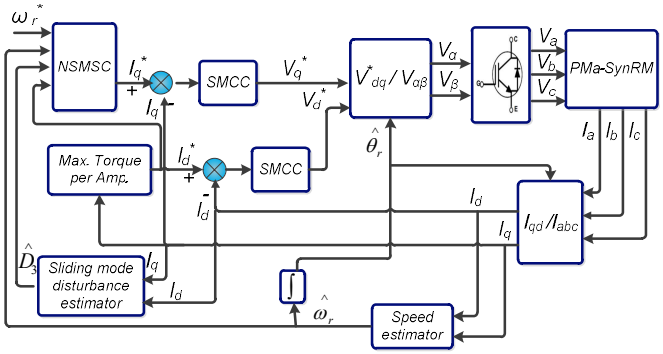

Fig. 1. The encoderless PMa-SynRM drive system with the SMCCs, sliding mode disturbance estimator, and the NSMSC.

The paper structure is prepared as follows: the mathematical representation of the PMa-SynRM is derived in Section II. Section III presents the detailed sliding surface design. The design of the PMa-SynRM nonlinear sliding mode speed controller is presented in Section IV. Section V introduces the design of the uncertainties' estimator. Section VI presents the design of the super-twisting sliding mode *dq*-axis current controllers. The experimental verification of the proposed encoderless PMa-SynRM with the NSMSC is introduced in Section VII and Section VIII finally concludes the paper.

II. The PMa-SynRM Mathematical Representation

A. PMa-SynRM Dynamic Representation

The dynamic representation of the 3-phase PMa-SynRM in the *dq*-frame is represented by:

$$V_q = RI_q + P\omega_r L_d I_d + P\omega_r \lambda_f + L_q \frac{dI_q}{dt} \tag{1}$$

$$V_d = RI_d - P\omega_r L_q I_q + L_d \frac{dI_d}{dt} \tag{2}$$

The PMa-SynRM electromagnetic torque in the *dq*-frame can be expressed as:

$$T_e = 1.5 \times P \times \left[\lambda_f I_q + (L_d - L_q) I_d I_q \right] \tag{3}$$

The mechanical representation of the PMa-SynRM can be expressed by:

$$T_e = T_L + J\frac{d\omega_r}{dt} + F\omega_r \tag{4}$$

Via substituting (3) into (4), the rotor angular speed of the PMa-SynRM can be expressed by (5):

$$\frac{d\omega_r}{dt} = \frac{1.5P\lambda_f I_q}{J} + \frac{1.5P(L_d - L_q)I_d I_q}{J} - \frac{F}{J}\omega_r - \frac{T_L}{J} \tag{5}$$

From (1)-(5), the PMa-SynRM dynamic model can be expressed by (6):

$$\begin{cases} \dfrac{dI_q}{dt} = -k_1 I_q - k_2\omega_r + k_3 V_q - k_4\omega_r I_d \\ \dfrac{dI_d}{dt} = -k_5 I_d + k_6 V_d + k_7\omega_r I_q \\ \dfrac{d\omega_r}{dt} = k_8 I_q - k_9\omega_r - k_{10}T_L + k_{11} I_d I_q \end{cases} \tag{6}$$

where the gains k_1-k_{11} are defined as follows: $k_1=R/L_q$, $k_2=P\lambda_f/L_q$, $k_3=1/L_q$, $k_4=PL_d/L_q$, $k_5=R/L_d$, $k_6=1/L_d$, $k_7=PL_q/L_d$, $k_8=1.5\ P\lambda_f/J$, $k_9=F/J$, $k_{10}=1/J$, and $k_{11}=1.5P(L_d-L_q)/J$.

By considering the system uncertainties e.g. external disorders and the PMa-SynRM parameter disparities, thus, (6) can be expressed by (7):

$$\begin{cases} \dfrac{dI_q}{dt} = -k_1 I_q - k_2\omega_r + k_3 V_q - k_4\omega_r I_d - k_{12}D_1 \\ \dfrac{dI_d}{dt} = -k_5 I_d + k_6 V_d + k_7\omega_r I_q - k_{13}D_2 \\ \dfrac{d\omega_r}{dt} = k_8 I_q - k_9\omega_r - k_{10}T_L + k_{11} I_d I_q - k_{14}D_3 \end{cases} \tag{7}$$

where D_1, D_2, *and* D_3 denote the uncertain components, which signify the PMa-SynRM parameter disparities along with the external disorders. These uncertain components are unidentified. Nevertheless, they are supposed to be bounded, e.g., there exist the constants μ_1, μ_2, and μ_3 that fulfill $|D_1| \le \mu_1$, $|D_2| \le \mu_2$ and $|D_3| \le \mu_3$. These suppositions are realistic as the motor parameters disparities cannot be infinite.

B. State Representation of PMa-SynRM

The state space variables of the PMa-SynRM can be represented by (8):

$$X_1 = \omega_r - \omega_D, X_2 = \frac{dX_1}{dt}, X_3 = I_d - I_D \tag{8}$$

where ω_D and I_D denote the desired values of rotor speed and d-axis current, respectively.

For the PMa-SynRM, the reluctance torque exists as L_q is greater than L_d. If I_D is retained at zero, thus, it is not conceivable to use the potential reluctance torque. Consequently, for maximizing the PMa-SynRM torque generation throughout the constant torque region as well as increasing the motor efficiency, thus, the armature current should be controlled via utilizing the maximum torque per ampere trajectory operation. Therefore, I_D can be represented by (9)

$$I_D = -\frac{(L_q - L_d)}{\lambda_f} {I_q}^2 \tag{9}$$

Via taking the derivative of (8) as well as using (7), one gets:

$$\frac{dX_1}{dt} = X_2$$

$$\begin{aligned} \frac{dX_2}{dt} &= -k_8k_2X_1 - k_9X_2 + k_8k_3V_q - k_8k_4I_d\omega_r \\ &\quad - k_8k_4\omega_D - k_9\frac{d\omega_D}{dt} + k_{11}\left[\frac{dI_d}{dt}I_q + \frac{dI_q}{dt}I_d\right] \\ &\quad - k_8k_1I_q - k_8k_3D_2 - k_{10}\frac{dD_1}{dt} - \frac{d^2\omega_D}{dt^2} \\ \frac{dX_3}{dt} &= -k_5X_3 + k_6V_d + k_7\omega_rI_q - k_6D_3 - k_5I_D - \frac{dI_D}{dt} \end{aligned} \tag{10}$$

So, both (11) and (12) can be formulated as follows:

$$\begin{aligned} N_1 &= -k_8k_2\omega_D - k_8k_4I_D\omega_r - k_9\frac{d\omega_D}{dt} \\ &\quad + k_{11}\left[\frac{dI_d}{dt}I_q + \frac{dI_q}{dt}I_d\right] - k_8k_1I_q \\ &\quad - k_8k_3D_2 - k_{10}\frac{dD_1}{dt} - \frac{d^2\omega_D}{dt^2} \end{aligned} \tag{11}$$

$$N_2 = -k_6D_3 + k_7\omega_rI_q - k_5I_D - \frac{dI_D}{dt} \tag{12}$$

From (11) and (12), (10) can be rewritten as:

$$\begin{cases} \dfrac{dX_1}{dt} = X_2 \\ \dfrac{dX_2}{dt} = k_8k_2X_1 - k_9X_2 + k_8k_3V_q + N_1 \\ \dfrac{dX_3}{dt} = -k_5X_3 + k_6V_d + N_2 \end{cases} \tag{13}$$

Based on (13), the PMa-SynRM dynamic model can be represented in the state space form by (14):

$$\frac{dX}{dt} = MX + WU + N \tag{14}$$

where $X=[X_1 \quad X_2 \quad X_3]^T$,

$$M = \begin{bmatrix} M_{11} & M_{12} & M_{13} \\ M_{21} & M_{22} & M_{23} \\ M_{31} & M_{32} & M_{33} \end{bmatrix} = \begin{bmatrix} 0 & 1 & 0 \\ k_8k_2 & -k_9 & 0 \\ 0 & 0 & -k_5 \end{bmatrix},\ W = \begin{bmatrix} 0 & 0 \\ 1 & 0 \\ 0 & 1 \end{bmatrix},$$

$$U = \begin{bmatrix} U_1 \\ U_2 \end{bmatrix} = \begin{bmatrix} k_8k_3V_q \\ k_6V_d \end{bmatrix},\ N = \begin{bmatrix} 0 \\ N_1 \\ N_2 \end{bmatrix}$$

III. THE SLIDING SURFACE DESIGN

A. The Sliding Surface Structure

Through this paper, the sliding surface, which is nonlinear, is structured via utilizing the variable damping principle perception. When the damping ratio of the system is altered from its original value to the ultimate high value, the transient-state of the drive performance can be rapid without overshoot whereas the probabilities of a singularity can be pointedly minimized [16]-[18]. Thus, the PMa-SynRM dynamic model can be rewritten by (15):

$$\begin{cases} \dfrac{dX_1}{dt} = X_2 \\ \dfrac{dX_2}{dt} = M_{21}X_1 + M_{22}X_2 + U_1 + N_1 \\ \dfrac{dX_3}{dt} = M_{33}X_3 + U_2 + N_2 \end{cases} \tag{15}$$

And the sliding surface can be represented by (16):

$$\sigma=\begin{bmatrix}\sigma_1\\ \sigma_2\end{bmatrix}=S_X=\begin{bmatrix}S_{1X}\\ S_{2X}\end{bmatrix}=\begin{bmatrix}B_{11}-\delta(y)M_{12}b & 1 & 0\\ B_{21}-\delta(y)M_{13}b & 0 & 1\end{bmatrix}$$
$$X=\begin{bmatrix}B_{11}-\delta(y)b & 1 & 0\\ B_{21} & 0 & 1\end{bmatrix}X=\begin{bmatrix}(B_{11}-\delta(y)b)X_1+X_2\\ B_{21}X_1+X_3\end{bmatrix} \quad (16)$$

where $B = [B_{11}\ B_{21}]^T$ represents a constant matrix that can be designed based on the damping ratio ζ_1 along with the settling time t_{set}. Meanwhile, b denotes a positive constant, which is selected based on the target ultimate damping ratio ζ_2 and it fulfills this condition:

$$(M_{11}-B^T M_1^T)b+b(M_{11}-M_1B)=-H \quad (17)$$
$$B^T M_1^T b+b(M_1B)=H \quad (18)$$

where H denotes a positive weighting constant and $M_1 = [M_{12}\ M_{13}] = [1\ 0]$.

According to (18), it can be noted that this equation is an algebraic Lyapunov equation, which is mandatory for ensuring the stability of the proposed approach. The system control output can be represented by:

$$y=CX=\begin{bmatrix}1 & 0 & 0\end{bmatrix}X \quad (19)$$

The function $\delta(y)$ choice should fulfill the condition when the output alters from the starting point to the origin, the function $\delta(y)$ value will decrease from zero or a very small value to $-\alpha$ (α represents a positive scalar). Thus, this condition will make the sliding surface of (16) nonsingular. Moreover, $\delta(y)$ should have the 1st degree differential equation in y. Through this paper, $\delta(y)$ is chosen according to [19] with this form:

$$\delta(y)=-\alpha e^{-ly^2} \quad (20)$$

where l denotes a positive scalar, which should be large enough for guaranteeing a small initial value of $\delta(y)$.

The stability analysis of (16) can be proved via this theory.

Theory#1: Suppose a matrix B, which is defined by $(M_{11} - M_1B)$ is stable and a positive definite matrix b, which is selected according to the target ultimate damping ratio ζ_2. Moreover, it accomplishes the condition in (16) with $\delta(y)$ identified via (20). Consequently, the nonlinear sliding surface expressed via (16) will be stable.

Theory#1Proof: Based on the standard SMC approach introduced by [18] and the sliding mode, $\sigma = d\sigma/dt = 0$, thus, according to (13), one gets:

$$\begin{cases}X_2=-[B_{11}-\delta(y)b]X_1\\ X_3=-B_{21}X_1\end{cases} \quad (21)$$

According to (21), the PMa-SynRM dynamics of (13) can be expressed by (22):

$$\frac{dX_1}{dt}=-[B_{11}-\delta(y)b]X_1 \quad (22)$$

Based on (22), Lyapunov function is expressed by (23):

$$V(X)=bX_1^2 \quad (23)$$

The derivative of $V(X)$ and (22) can be expressed by (24):

$$\frac{dV(X)}{dt}=2bX_1\frac{dX_1}{dt}=-2bX_1[B_{11}-\delta(y)b]X_1 \quad (24)$$
$$=2X_1^2[-bB_{11}+\delta(y)b^2]$$

The condition denoted via (18) indicates that:

$$\frac{dV(X)}{dt}=X_1^2[-H+2\delta(y)b_2] \quad (25)$$

Based on (25), the function $\delta(y)$ properties ensure that it is a negative function. Furthermore, the dynamics of the sliding mode in (22) or the sliding surface in (16) is asymptotically stable.

B. The Design of the Sliding Surface Parameters

According to (15), the sliding surface has nonlinear and linear components. $\delta(y)$ through the nonlinear part alters its value from 0 to $-\alpha$ in case the output alters from the initial state to the origin. This reduction allows the system damping ratio increase from the ζ_1 to the ultimate value ζ_2. For the system in (26) and throughout the initial-state and via selecting the factor l with a high value, $\delta(y)$ has a small value and can be neglected.

$$\frac{dX_1}{dt}=[M_{11}-M_1B+\delta(y)(M_{12}^2+M_{13}^2)b]X_1 \quad (26)$$
$$=-[B_{11}-\delta(y)b]X_1$$

The damping ratio can be identified via B. Accordingly, the matrix B can be designed with a low damping ratio ζ_1. Through this paper, the matrix B is identified via the pole placement technique with known damping ratio along with initial settling time. Throughout the steady-state operation, the output approaches the origin point and the function $\delta(y)$ reaches its ultimate value $\delta(y) = -\alpha$. Consequently, the nominal reduced-order dynamics of (22) can be expressed by:

$$\frac{dX_1}{dt}=[M_{11}-M_1B-\alpha(M_{12}^2+M_{13}^2)b]X_1$$
$$=-[M_{11}-M_1(B+\alpha M_1^T b)]X_1 \quad (27)$$
$$=(M_{11}-M_1m)X_1=-M_1mX_1$$

where

$$m=B+\alpha M_1^T b \quad (28)$$

or

$$M_1^T b-\frac{m-B}{\alpha}=0 \quad (29)$$

The parameters m can be calculated like the calculation of B for the ultimate damping ratio ζ_2. In addition, for the closed-loop system stability, the matrix b should fulfill the condition (17). Moreover, for realizing the target damping ratio, the matrix b needs to fulfill (29). Nevertheless, it is hard to obtain a matrix b that fulfills both (17) and (29). Consequently, the condition of (29) can be updated by (30):

$$\left\|M_1^T b-\frac{m-B}{\alpha}\right\|\le\gamma \quad (30)$$

where γ is greater than zero and is scalar. Via employing the Schur complement formula, the condition identified via (30) can be expressed in this form:

$$\begin{bmatrix}\gamma I & M_1^T b-\frac{m-B}{\alpha}\\ \left(M_1^T b-\frac{m-B}{\alpha}\right)^T & \gamma I\end{bmatrix}=0 \quad (31)$$

where I denotes the identity matrix. Based on (31), the design

target is to find the matrix b that reduces γ such that:

$$\begin{cases} b \succ 0 \\ B^T M_1{}^T b + b M_1 B \succ 0 \end{cases} \tag{32}$$

$$\begin{pmatrix} \gamma I & M_1{}^T b - \dfrac{m-B}{\alpha} \\ \left(M_1{}^T b - \dfrac{m-B}{\alpha}\right)^T & \gamma I \end{pmatrix} \succ 0 \tag{33}$$

IV. The Design of the PMa-SynRM Nonlinear Sliding Mode Speed Controller

In this paper, the nonlinear sliding mode speed control law is formulated for (14) via utilizing the nonlinear sliding surface in (16). The speed controller should ensure the attainment condition for guaranteeing that the system trajectory approaches the sliding surface from any initial value and afterwards slides laterally the sliding surface to the origin. This controller is designed based on theory#2.

Theory#2: Supposing that the uncertain parameter N is bounded via a constant as well as there exists some positive constant ε such that $\varepsilon \geq ||S||||N||$. The nonlinear feedback control law can be expressed by (34):

$$U = -\left(SMX + O\sigma + \varepsilon sign(\sigma) + X\frac{dS}{dt} \right) \tag{34}$$

where O denotes a positive scalar, σ denotes the nonlinear sliding surface expressed via (16). Afterwards, the uncertain system state in (15) will approach to zero.

Theory#2 Proof: Based on the standard SMC in [18], the sliding surface will reach zero in a finite amount of time in case the sliding condition $\sigma^T d\sigma/dt$ is less than zero and guaranteed for $\forall\sigma(t) \neq 0$. Based on (14), (16), and (34), the approaching condition is expressed by (35):

$$\begin{aligned} \frac{\sigma^T d\sigma}{dt} &= \sigma^T \left[S\frac{dX}{dt} + X\frac{dS}{dt} \right] \\ &= \sigma^T \left[S(MX + WU + N) + X\frac{dS}{dt} \right] \\ &= \sigma^T \left[SMX + SWU + SN + X\frac{dS}{dt} \right] \end{aligned} \tag{35}$$

where $SW=I$. Eq. (35) can be rewritten by:

$$\begin{aligned} \frac{\sigma^T d\sigma}{dt} &= \sigma^T \left[SMX + U + SN + XdS/dt \right] \\ &= \sigma^T [SMX - SMX - O\sigma - \varepsilon\, sign(\sigma) \\ &\quad - XdS/dt + SN + XdS/dt] \\ &= \sigma^T (-O\sigma - \varepsilon sign(\sigma) + SN) \\ &\leq -O\|\sigma\|^2 - \varepsilon(|\sigma_1| + |\sigma_2|) + |\sigma_1|.|S_1 N| + |\sigma_2|.|S_2 N| \\ &\leq -O\|\sigma\|^2 - \varepsilon(|\sigma_1| + |\sigma_2|) + |\sigma_1|.\|S_1\|.\|N\| + |\sigma_2|.\|S_2\|.\|N\| \\ &\leq -O\|\sigma\|^2 - \varepsilon(|\sigma_1| + |\sigma_2|) + \|S\|.\|N\|(|\sigma_1| + |\sigma_2|) \\ &\leq -O\|\sigma\|^2 \end{aligned} \tag{36}$$

Based on (36), the stable sliding motion is induced through a finite amount of time. Afterwards it attains the theory#2 proof.

Based on (34), the control law U has the entire derivative of the output. Through this paper, the derivative can be obtained via employing the robust differentiator of Utkin in [19]. Moreover, the ε value in (34) is an indefinite constant. This value is attained via this adaptation law:

$$\frac{d\hat{\varepsilon}}{dt} = \frac{\sigma^T sign(\sigma)}{\beta} \tag{37}$$

where β denotes a positive scalar. Via employing (37), the controller in (34) can be expressed by:

$$U = -\left(SMX + O\sigma + \hat{\varepsilon}\, sign(\sigma) + X\frac{dS}{dt} \right) \tag{38}$$

The validation of the control law of (38) along with the adaptation law of (37) is proved via Lyapunov theory. The adaptation error can be expressed by (39):

$$\tilde{\varepsilon} = \varepsilon_d - \hat{\varepsilon} \tag{39}$$

where ε_d is an indefinite real value of ε, and $\varepsilon_d \geq$ ||S||||N||. Lyapunov function can be expressed by (40):

$$V_1 = 0.5\sigma^T\sigma + 0.5\beta\tilde{\varepsilon}^2 \tag{40}$$

The derivative of V_1 and (39) can be expressed by (41):

$$\frac{dV}{dt}_1 = \sigma^T \frac{d\sigma}{dt} + \beta\frac{d\tilde{\varepsilon}}{dt}\tilde{\varepsilon} \tag{41}$$

Based on (36), (39), and (40), one gets:

$$\begin{aligned} \frac{dV_1}{dt} &= \sigma^T(-O\sigma - \hat{\varepsilon}\, sign(\sigma) + SN) - \beta\frac{d\hat{\varepsilon}}{dt}\tilde{\varepsilon} \\ &= \sigma^T(-O\sigma - \varepsilon_d sign(\sigma) + SN) + \tilde{\varepsilon}\sigma^T sign(\sigma) - \beta\frac{d\hat{\varepsilon}}{dt}\tilde{\varepsilon} \\ &\leq -O\|\sigma\|^2 + \tilde{\varepsilon}(\sigma^T sign(\sigma) - \beta\frac{d\hat{\varepsilon}}{dt}) \end{aligned} \tag{42}$$

Thus, (37) ensures that:

$$\frac{dV_1}{dt} \leq -O\|\sigma\|^2 \leq 0 \tag{43}$$

V. The Uncertainties Estimator Design

Based on (7) and (13), the nonlinear SMC has system uncertainties D_3 along with load torque disorders T_L. These indefinite disorders can make the PMa-SynRM speed unstable throughout the transient-state operation. Furthermore, they can make unpredicted errors throughout the steady-state. So, in the PMa-SynRM speed tracking control, knowing these disorders is obligatory. Hence, a simple sliding mode estimator is employed for estimating the system uncertainties D_3 along with the load torque disorders T_L.

According to the PMa-SynRM rotor speed representation of (7) and for designing a sliding mode uncertainties estimator, the sliding surface can be expressed by (44):

$$\sigma_\omega = \omega_r - \hat{\omega}_r \tag{44}$$

where $\hat{\omega}_r$ denotes the estimated rotor speed of the PMa-SynRM and can be obtained from (45):

$$\frac{d\hat{\omega}_r}{dt} = k_8 I_q - k_9\omega_r + k_{11} I_d I_q + \rho\,\mathrm{sgn}(\omega_r - \hat{\omega}_r) \tag{45}$$

where ρ is greater than zero. The error dynamics of the sliding mode estimator can be obtained from (46):

$$\frac{d\sigma_\omega}{dt} = \frac{d\omega_r}{dt} - \frac{d\hat{\omega}_r}{dt} = -k_{14}D_3 - \rho\,\mathrm{sgn}(\sigma_\omega) \tag{46}$$

Based on the standard sliding mode approach in [19], the steady-state, $\sigma_\omega=d\,\sigma_\omega/dt=0$. Via utilizing (40), one gets:

$$k_{14}D_3 \approx -\rho\,\mathrm{sgn}(\sigma_\omega) \tag{47}$$

The estimated uncertainties can be obtained by (48):

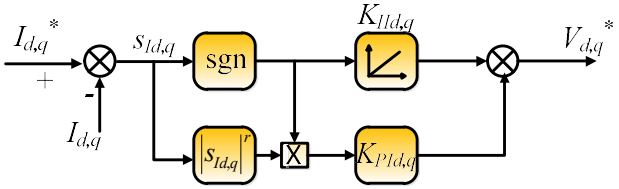

Fig. 2. The general structure of the ST-SMCC for the *dq*-axis currents.

$$\hat{D}_3 = \frac{-\mathrm{sgn}(\sigma_\omega)}{k_{14}(1+S\tau_f)} \tag{48}$$

where S denotes the Laplace variable, and τ_f represents an adequately small filter time constant.

VI. The Design of The Super-Twisting Sliding Mode *DQ*-Axis Current Controllers

In this paper, both the *d*-axis and *q*-axis currents are controlled via the ST-SMCC. The *d*-axis ST-SMCC controller is utilized for producing the V_d^*. Meanwhile, the *q*-axis ST-SMCC controller is utilized for producing the V_q^*.

Fig. 2 depicts the general structure of the *dq*-axis ST-SMCCs. For the *d-q* axis currents, the switching function $s_{Id,q}$, which represents the difference between the $I_{d,q}^*$ and $I_{d,q}$ can be expressed by (49):

$$s_{Id,q} = I_{d,q}^* - I_{d,q} \tag{49}$$

where $s_{Id,q}$ denotes the switching function. This controller is utilized for producing the V_d^* and V_q^*, respectively. The *d-q* axis ST-SMCCs can be represented by (50) and (51):

$$V_{d,q}^* = K_{PId,q}\left|s_{Id,q}\right|^r \mathrm{sgn}\left(s_{Id,q}\right) + V_{d,q1}^* \tag{50}$$

$$\frac{dV_{d,q1}^*}{dt} = K_{IId,q}\,\mathrm{sgn}\left(s_{Id,q}\right) \tag{51}$$

where r represents the exponent, which can be distinct for ST-SMCC. Meanwhile, $K_{IId,q}$ and $K_{PId,q}$ designate the *d-q* axis ST-SMCCs integral and proportional gains, respectively. The dynamics and response of the ST-SMCCs can be adjusted via varying the exponent r along with ST-SMCCs proportional and integral gains.

VII. Experimental Results

In order to check the effectiveness of the proposed speed estimation and the NSMSC approach, a conventional linear sliding mode speed controller (LSMSC) is employed instead for controlling the three-phase PMa-SynRM (Table I). LSMSC utilizes linear sliding surfaces that may not be the proper solution for the global dynamic property of nonlinear systems. Consequently, sliding cannot occur because of the actuator saturation and the instability may be induced if the error is large. Moreover, linear sliding surfaces can cause large chattering in digital implementation. These problems can be solved via exchanging linear sliding surfaces with nonlinear sliding surfaces as indicated in this paper. Therefore, the performance of the proposed NSMSC is compared with the LSMSC and the detailed comparison is presented in this section.

TABLE I
THE PMA-SYNRM SPECS

Nominal power (kW)	1.1	Number of pair-poles	3
Nominal voltage (V)	400	Inertia of the motor and load (kg·m^2)	0.0036
Nominal speed (rpm)	3000	Friction coefficient (N·m/rad/sec)	0.0011
Nominal current (A)	2.3	Nominal torque (N·m)	4.1
Stator resistance (Ω/phase)	6.2	PM flux (Wb)	0.305
d-axis inductance (mH/phase)	25.025	*q*-axis inductance (mH/phase)	40.17

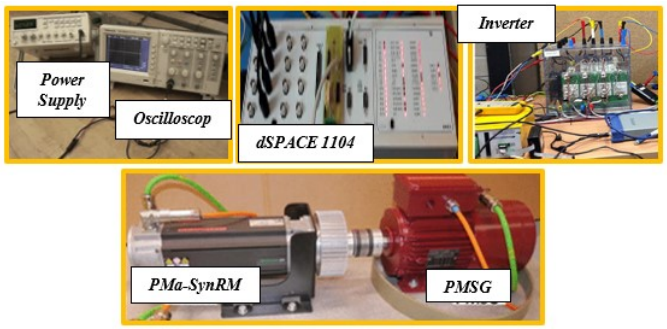

Fig. 3. The hardware implementation for the experimental validation setup of PMa-SynRM drive system.

Fig. 3 depicts the lab setup for validating the proposed NSMSC for the encoderless PMa-SynRM with specification in Table I via utilizing dSPACE 1104. In order to check the effectiveness of the proposed encoderless approach, an optical encoder is mounted on the PMa-SynRM shaft to measure the rotor speed (Speed-meas). The estimated speed is realized via reading the current sensors of LA 25-NP for measuring I_a, I_b, I_c using, which are converted to I_d and I_q and through using these readings and using (45), the estimated speed can be obtained. The pulse width modulation converter is employed for driving the system. Both 10 and 1 kHz sampling frequencies are chosen for the current and speed loops, respectively. The detailed coefficients of the proposed NSMSC and the LSMSC are as follows: ρ=7000, τ_f= 0.02, ζ_1= 1, B= [188.7 0]^T, H= 0.001, b= 4.2×10^{-6}, α=500, l=30, O= 300, β= 2000, k_1= 154.34, k_2=22.78, k_3= 24.89, k_4= 1.87, k_5= 247.75, k_6= 39.96, k_7= 4.82, k_8= 381.25, k_9= 0.305, k_{10}= 277.78, k_{11}= 18931.25.

A. The NSMSC Performance under Different Speed Command and Full Load

Fig. 4 depicts the PMa-SynRM performance using the proposed speed estimation and the NSMSC versus the LSMSC throughout different speed references along with a full load condition. As depicted, the transient response of the LSMSC is more oscillatory than the proposed NSMSC throughout the different speed references condition. The steady-state response of the proposed NSMSC has better performance with fewer ripples than the LSMSC. In addition, the torque ripples via the NSMSC are less than the LSMSC. The PMa-SynRM transient response analysis with the (%) overshoot and settling time of the motor speed for both the NSMSC and LSMSC is summarized in Table II. For high

speed range (~50-100%) of rated speed, the proposed NSMSC has less overshoot (~28.1-30.8%) compared to LSMSC (~15.4-28.7%). Nevertheless, LSMSC has less settling time (~0.081-1.277 sec) compared to NSMSC (~0.421-0.758 sec). For low speed range (~12.5%) of rated speed, the proposed NSMSC has quicker performance with settling time range (~0.571-1.008 sec) compared to the LSMSC (~0.176-1.564 sec).

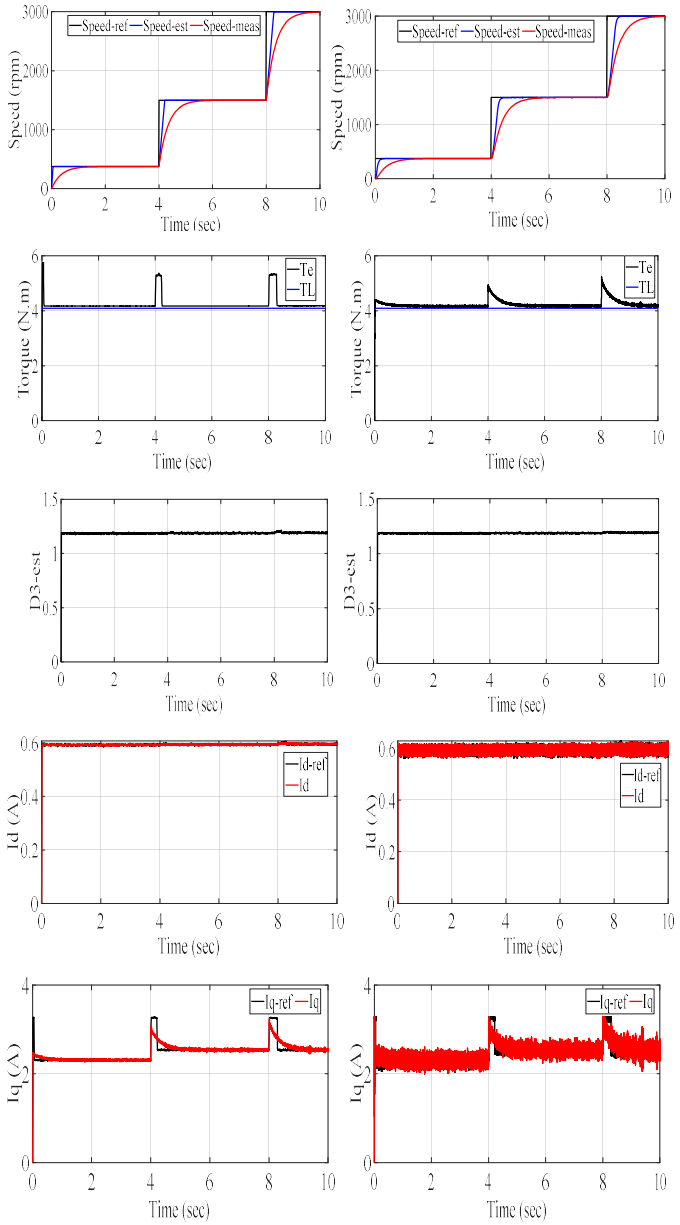

(a) (b)

Fig. 4. The PMa-SynRM response using the proposed NSMSC and conventional LSMSC at different speed references and full load condition. (a) Using the NSMSC. (b) Using the LSMSC.

TABLE II
THE NSMSC RESPONSE VERSUS THE LSMSC UNDER DIFFERENT SPEED COMMANDS AND FULL LOAD TORQUE CONDITION

Controller	ω_r^*	T_{ripple}%	*Settling time (sec)*
Proposed NSMSC	12.5%ω_{rated}	15.7	0.571
	50%ω_{rated}	14.2	0.421
	100%ω_{rated}	8.5	0.758
Conventional	12.5%ω_{rated}	20.7	0.176
LSMSC	50%ω_{rated}	35.4	0.081
	100%ω_{rated}	40.2	1.277

B. The NSMSC Performance Throughout Electrical Parameters Disparities

Fig. 5 depicts the 3-phase PMa-SynRM response via the NSMSC versus the LSMSC throughout +50% increase in the stator resistance along with +50% increase in L_q at t=5 sec and rated full speed condition. As depicted, the proposed NSMSC proved its robustness alongside the electrical parameters' alteration in the PMa-SynRM stator resistance along with the L_q. Table III summarizes the response analysis of the PMa-SynRM based on the mean torque and the torque ripples of both controllers. It can be noticed that the proposed NSMSC

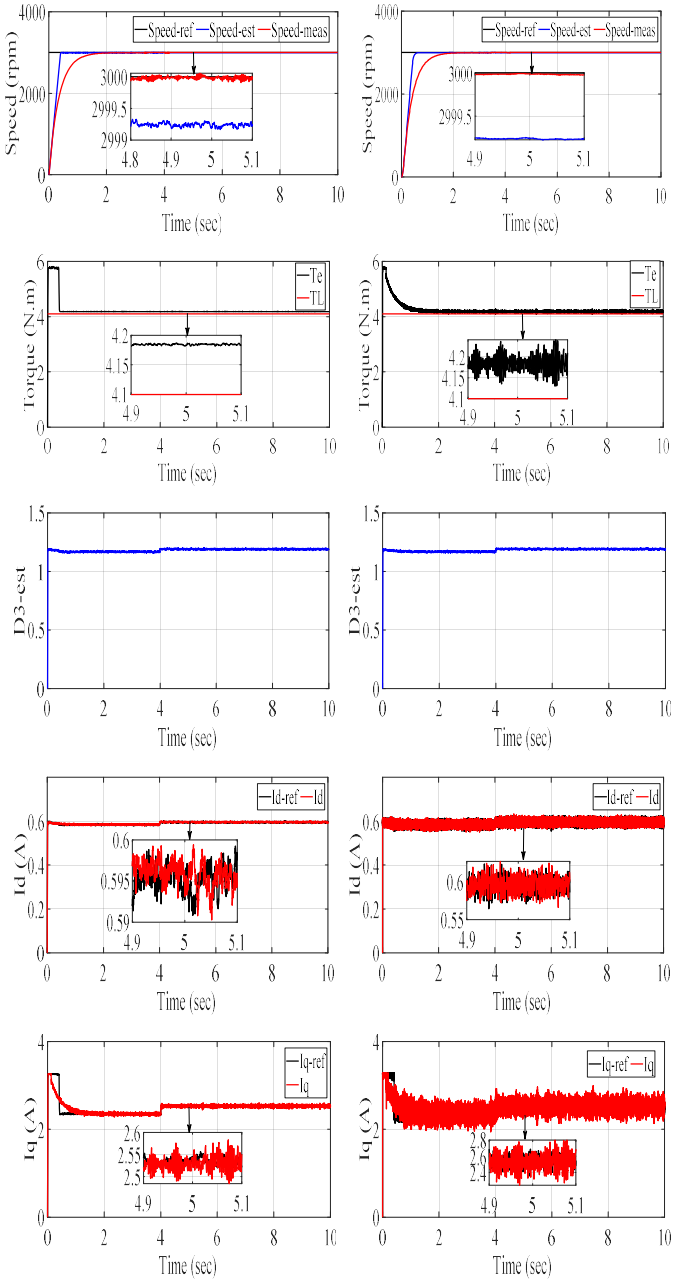

(a) (b)

Fig. 5. The PMa-SynRM response using the proposed NSMSC and conventional LSMSC at electrical parameter disparities condition. (a) Using the NSMSC. (b) Using the LSMSC.

TABLE III
THE NSMSC RESPONSE VERSUS THE LSMSC UNDER ELECTRICAL PARAMETERS DISPARITIES

Controller	ω_r^*	T_{ripple} %	T_{mean} (N·m)
Proposed NSMSC	100%ω_{rated}	0.16	1.021
Conventional LSMSC	100%ω_{rated}	7.5	1.016

has less torque ripples (~0.16%) compared to the LSMSC (~7.5%).

C. The NSMSC Performance under Mechanical Parameter Variations

Fig. 6 depicts the PMa-SynRM response via employing the proposed NSMSC versus the LSMSC throughout +100% increase in motor inertia and +150% increase in the friction coefficient at t=5 sec and full rated speed condition. Table IV summarizes the response analysis of the PMa-SynRM through via employing the proposed NSMSC versus the LSMSC. As depicted in Fig. 6, the proposed NSMSC proved its robustness alongside the PMa-SynRM mechanical parameter alteration. Moreover, the proposed NSMSC has less torque ripples (~0.10%) compared to the LSMSC (~5.6%). In addition, the NSMSC has higher mean torque (~4.016 N·m) compared to the LSMSC (~4.011 N·m). It is worth restating that the proposed NSMSC has attained more robust response alongside the parameter uncertainties.

TABLE IV
THE NSMSC RESPONSE VERSUS THE LSMSC UNDER MECHANICAL PARAMETERS DISPARITIES

Controller	ω_r^*	T_{ripple} %	T_{mean} (N·m)
Proposed NSMSC	100%ω_{rated}	0.1	4.016
Conventional LSMSC	100%ω_{rated}	5.6	4.011

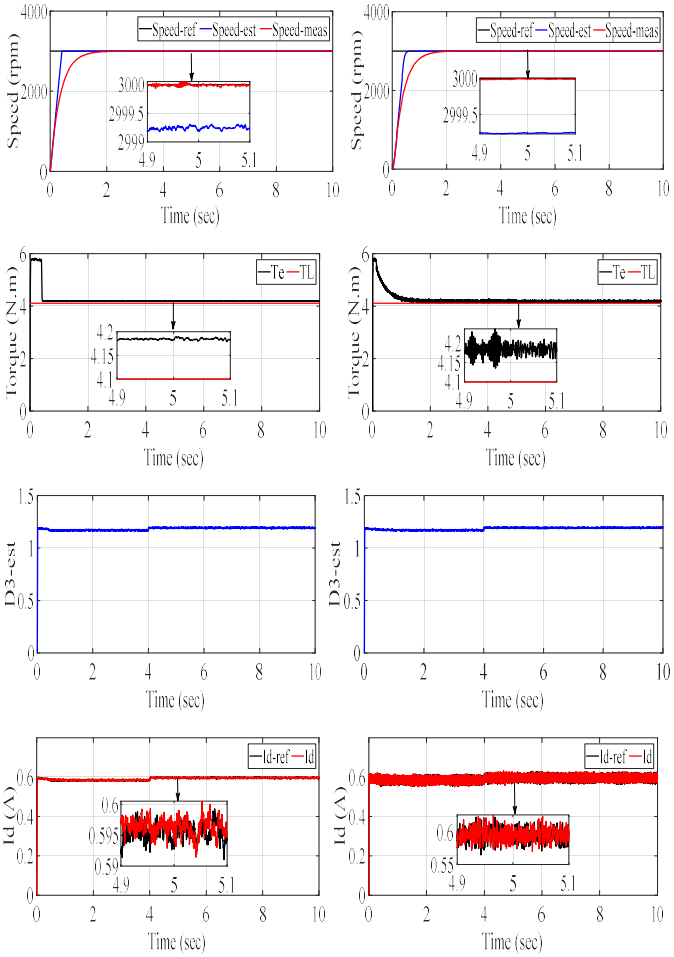

(a) (b)

Fig. 6. The PMa-SynRM response using the proposed NSMSC and conventional LSMSC at mechanical parameter disparities condition. (a) Using the NSMSC. (b) Using the LSMSC.

D. The NSMSC Performance under Load Disturbance Condition

Fig. 7 depicts the PMa-SynRM response via employing the proposed NSMSC versus the LSMSC at full rated speed with load disturbance condition at t=3 sec with full load torque and then half of the load torque at t=7 sec. Table V summarizes the response analysis of the PMa-SynRM through via employing the proposed NSMSC versus the LSMSC. As depicted in Fig. 7, the proposed NSMSC proved its robustness alongside the load disturbance condition. Moreover, the proposed NSMSC has less torque ripples (~1.2%) compared to the LSMSC (~7.2%). In addition, the NSMSC has higher mean torque (~6.1 N·m) compared to the LSMSC (~3.2 N·m). It is worth restating that the proposed NSMSC has attained more robust

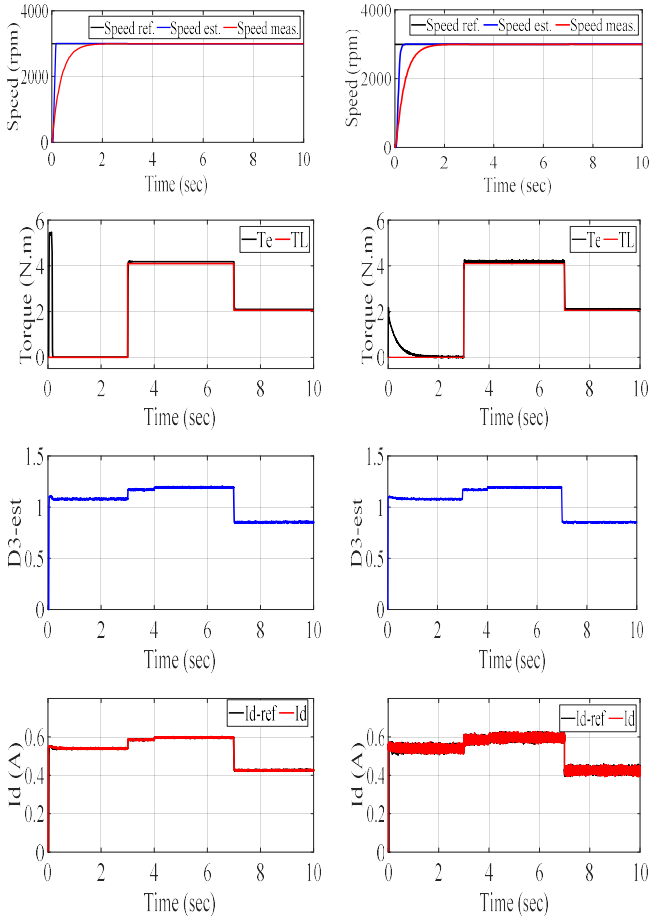

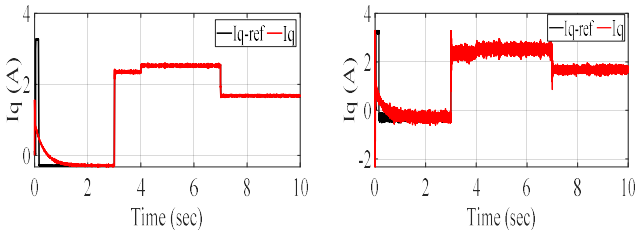

Fig. 7. The PMa-SynRM response using the proposed NSMSC and conventional LSMSC at load disturbance condition. (a) Using the NSMSC. (b) Using the LSMSC.

TABLE V
THE NSMSC RESPONSE VERSUS THE LSMSC UNDER LOAD DISTURBANCE CONDITION

Controller	ω_r^*	T_{ripple} %	T_{mean} (N·m)
Proposed NSMSC	100%ω_{rated}	1.2	6.1
Conventional LSMSC	100%ω_{rated}	7.2	3.2

response alongside the load disturbance condition.

VIII. CONCLUSIONS

In this paper, a realization of an adaptive gain tuning rule has been designed for the nonlinear sliding mode speed control so as to improve the dynamic performance and the robustness of the three-phase PMa-SynRM with considering the parameter uncertainties has been presented. A detailed real-time comparison between the proposed nonlinear sliding mode speed control versus the conventional linear sliding mode speed control has been introduced. This comparison was investigated throughout different speed references, electrical and mechanical parameters disparities, and load disturbance conditions. The proposed NSMSC gave better response as the system reliability increases and the entire cost minimizes. In addition, the proposed NSMSC has accomplished rapider transient performance at high speed condition. Furthermore, less torque ripples and higher mean torque has been attained via employing the proposed NSMSC. The intensive experimental validation results confirmed that the proposed NSMSC approach is more robust than the LSMSC to acute the PMa-SynRM mechanical and electrical parameters disparities and load disturbance conditions with excellent speed and current tracking performance and more robust dynamic performance and smaller steady-state errors.

REFERENCES

[1] A. Mohammadi and S. M. Mirimani. "Design of a Novel PM-Assisted Synchronous Reluctance Motor Topology Using V-Shape Permanent Magnets for Improvement of Torque Characteristic," *IEEE Transactions on Energy Conversion*, vol. 37, no. 1, pp. 424-432, March 2022.

[2] M. Degano *et al*., "Optimised Design of Permanent Magnet Assisted Synchronous Reluctance Machines for Household Appliances," *IEEE Transactions on Energy Conversion*, vol. 36, no. 4, pp. 3084-3095, Dec. 2021.

[3] B. Wang, J. Hu, W. Hua, and Z. Wang, "Fault Operation Analysis of a Triple-Redundant Three-Phase PMA-SynRM for EV Application," *IEEE Transactions on Transportation Electrification*, vol. 7, no. 1, pp. 183-192, Mar. 2021.

[4] M. Amin and G. A. A. Aziz, "Hybrid Adopted Materials in Permanent Magnet-Assisted Synchronous Reluctance Motor With Rotating Losses Computation," *IEEE Transactions on Magnetics*, vol. 55, no. 6, pp. 1-5, Jun. 2019.

[5] A. Nobahari, A. Vahedi, and R. Nasiri-Zarandi, "A Modified Permanent Magnet-Assisted Synchronous Reluctance Motor Design for Torque Characteristics Improvement," *IEEE Transactions on Energy Conversion*, vol. 37, no. 2, pp. 989-998, Jun. 2022.

[6] G. Feng, C. Lai, X. Tan, W. Peng, and N. C. Kar, "Multi-Parameter Estimation of PMSM Using Differential Model With Core Loss Compensation, *IEEE Transactions on Transportation Electrification*, vol. 8, no. 1, pp. 1105-1115, Mar. 2022.

[7] Q. Wang, G. Zhang, G. Wang, C. Li, and D. Xu, "Offline Parameter Self-Learning Method for General-Purpose PMSM Drives With Estimation Error Compensation," *IEEE Transactions on Power Electronics*, vol. 34, no. 11, pp. 11103-11115, Nov. 2019.

[8] Z. Li, G. Feng, C. Lai, D. Banerjee, W. Li, and N. C. Kar, "Current Injection-Based Multi-parameter Estimation for Dual Three-Phase IPMSM Considering VSI Nonlinearity," *IEEE Transactions on Transportation Electrification*, vol. 5, no. 2, pp. 405-415, Jun. 2019.

[9] X. Li and R. Kennel, "General Formulation of Kalman-Filter-Based Online Parameter Identification Methods for VSI-Fed PMSM," *IEEE Transactions on Industrial Electronics*, vol. 68, no. 4, pp. 2856-2864, Apr. 2021.

[10] Z. Wang, J. Chai, X. Xiang, X. Sun, and H. Lu, "A Novel Online Parameter Identification Algorithm Designed for Deadbeat Current Control of the Permanent-Magnet Synchronous Motor," *IEEE Transactions on Industry Applications*, vol. 58, no. 2, pp. 2029-2041, Mar.-Apr. 2022.

[11] H. -C. Yeh and S. -M. Yang, "Phase Inductance and Rotor Position Estimation for Sensorless Permanent Magnet Synchronous Machine Drives at Standstill," *IEEE Access*, vol. 9, pp. 32897-32907, 2021.

[12] M. Amin and G. A. Abdel Aziz, "A Hardware-in-the-Loop Realization of a Robust Discrete-Time Current Control of PMa-SynRM for Aerospace Vehicle Applications," *IEEE Journal of Emerging and Selected Topics in Power Electronics*, vol. 7, no. 2, pp. 936-945, Jun. 2019.

[13] J. Xia, Z. Li, D. Yu, Y. Guo, and X. Zhang, "Robust Speed and Current Control With Parametric Adaptation for Surface-Mounted PMSM Considering System Perturbations," *IEEE Journal of Emerging and Selected Topics in Power Electronics*, vol. 9, no. 3, pp. 2807-2817, Jun. 2021.

[14] Y. Ma, D. Li, Y. Li, and L. Yang, "A Novel Discrete Compound Integral Terminal Sliding Mode Control With Disturbance Compensation For PMSM Speed System," *IEEE/ASME Transactions on Mechatronics*, vol. 27, no. 1, pp. 549-560, Feb. 2022.

[15] Y. Yao, Y. Huang, F. Peng, and J. Dong, "A Sliding-Mode Position Estimation Method With Chattering Suppression for LCL-Equipped High-Speed Surface-Mounted PMSM Drives," *IEEE Transactions on Power Electronics*, vol. 37, no. 2, pp. 2057-2071, Feb. 2022.

[16] M. M. Amin, F. F. M. El-Sousy, O. A. Mohammed, G. A. A. Aziz, and K. Gaber, "MRAS-Based Super-Twisting Sliding-Mode Estimator Combined With Block Control and DTC of Six-Phase Induction Motor for Ship Propulsion Application," *IEEE Transactions on Industry Applications*, vol. 57, no. 6, pp. 6646-6658, Nov.-Dec. 2021.

[17] J.-W. Jung et al., "A Nonlinear Sliding Mode Controller for IPMSM Drives with an Adaptive Gain Tuning Rule," *Journal of Power Electronics*, vol. 15, no. 3, pp. 753–762, May 2015.

[18] L. Yuan, Y. Jiang, L. Xiong, and P. Wang, "Sliding mode control approach with integrated disturbance observer for PMSM speed system," *CES Transactions on Electrical Machines and Systems*, early access, Jan. 17, 2023, doi: 10.30941/CESTEMS.2023.00009.

[19] L. Wu, Z. Lyu, Z. Chen, J. Liu and Y. Lu, "An Enhanced Sensorless Control Scheme for PMSM Drives Considering Self-inductance Asymmetry," *CES Transactions on Electrical Machines and Systems*, vol. 6, no. 4, pp. 384-392, Dec. 2022.

Ghada A. Abdel Aziz (Member, IEEE) received the B.Sc. and M.Sc. degrees in electrical power and machines engineering from Minofiya University, Egypt, in 2006 and 2009, respectively, and the Ph.D. degree in electrical power and machines engineering from Cairo University, Egypt, in 2015. Currently, she

is an associate professor at Electronics Research Institute (ERI) in Egypt. From 2006 to 2008, she was a TA with several academic institutions in Egypt. Since 2009, she joined the ERI, as a research assistant, where she has been a researcher since 2015. She was awarded as the best researcher at ERI due to her published papers at the IEEE, in 2018 and 2019, respectively. Her current research interests include control of electrical machines, electrical machines drives, fault-tolerant control, fault-tolerant design of the electric machine, and power electronics in renewable energy systems. She has a patent No. 30183, entitled "A method to detect the phase angle and frequency of the utility grid using the virtual power", which has been issued from the Scientific Research Academy in Egypt in February 2021.

Rehan Ali Khan received a Doctoral degree from the College of Electrical Engineering, Zhejiang University Hangzhou, P.R China. He did Master degree in Electronics and Communication from the University of Lahore, Pakistan in 2013 and Bachelor degree in Telecommunication Engineering from Balochistan University of Information Technology, Engineering and Management Sciences Quetta, Pakistan in 2010. He is working as an Assistant Professor at the Department of Electrical Engineering, University of Science and Technology Bannu, Pakistan since 2011. Research interests include Optimization, Computational Electromagnetics, Smart Grids and Wireless Communication.